Maxwell–Bloch dynamics and modulation instabilities in fiber lasers and amplifiers

Guido H. M. van Tartwijk and Govind P. Agrawal

The Institute of Optics and Rochester Theory Center, University of Rochester, Rochester, New York 14627

Received January 31, 1997; revised manuscript received March 24, 1997

We investigate analytically the occurrence of modulation instability in doped fiber lasers and amplifiers using a Maxwell–Bloch description for the dopants and without making the usual parabolic-gain approximation. We find a new modulation instability occurring near the Rabi frequency, which is not predicted by the conventional complex Ginzburg–Landau model. We discuss the implications of this new instability for fiber amplifiers and lasers and analyze the effects of the saturable host absorption on the laser instabilities. Atomic detuning is shown to significantly enhance the new modulation instability, in both the normal- and the anomalous-dispersion regimes. © 1997 Optical Society of America [S0740-3224(97)04610-9]

1. INTRODUCTION

The onset of instabilities in various kinds of lasers is generally studied by use of a rate-equation model based on the Maxwell–Bloch equations suitable for a two-level atomic system.[1] Such a model, often referred to as the (detuned) Lorenz–Haken model, includes atomic polarization dynamics and has been used extensively over the past two decades. Its use leads to the concept of the second laser threshold, defined as the pump level at which the continuous-wave (cw) operation of the laser becomes unstable through a Hopf bifurcation, resulting in a self-pulsing output. At higher pump levels the laser can enter into a chaotic regime through a period doubling or another route to chaos.[1,2]

The advent of fiber lasers during the late 1980's forces several changes to this standard model of laser instabilities, mainly because the optical fiber, acting as a host to the dopants, introduces group-velocity dispersion (GVD) and self-phase modulation (SPM), both of which must be incorporated for a proper description of the onset of instabilities in fiber lasers.[3] In fact, these two phenomena lead to an instability, known as the modulation instability (MI), even in an undoped and unpumped optical fiber.[4] It is therefore reasonable to expect that the presence of GVD and SPM in the host fiber would change the nature of instabilities in fiber lasers in comparison with other kinds of lasers (gas and solid-state lasers) that are well described by the standard Lorenz–Haken model. Apart from this propagation-based instability, several other explanations for the observed instabilities in rare-earth-doped fiber lasers have been reported. It was shown theoretically and experimentally that the existence of ion clusters in heavily Er-doped fiber lasers leads to single-mode cw or self-pulsing behavior, whereas the same model is also applicable to dual-wavelength or bipolarized lasers.[5,6] Other theories and experiments on Er-doped fiber lasers have shown self-pulsing, chaos, and antiphase dynamics between the different polarization eigenstates of the optical field.[7,8] The explanation for the self-pulsing behavior of Nd-doped fiber lasers has been reported to be driven by the dynamics of the two field-polarization eigenstates that depend on the birefringence of the fiber.[9,10] In this paper, however, we focus on the propagation-driven MI phenomenon, and do not consider any field-polarization dynamics.

In recent years, the MI phenomenon has been investigated in doped (active) fibers used to make lasers and amplifiers.[3,4,11,12] When doing so, one has to consider the nonlinear interaction of the dopants with the optical field. A natural choice is to model the dopants as a two-level system with an atomic polarization dephasing time T_2 and a population relaxation time T_1. By far, the most popular model employs the parabolic-gain approximation, leading to a complex Ginzburg–Landau (CGL) equation for the optical field.[3] One study showed that in erbium-doped fiber amplifiers,[11] the threshold for MI is considerably lowered compared with that for undoped fibers. Recently, Chen *et al.*[12] included gain dynamics (governed by T_1) as well as a fast saturable absorber in the model and discussed the implications of MI for passively mode-locked figure-eight lasers. The full atomic polarization dynamics (governed by T_2) has, however, been neglected so far.

In this paper we investigate the occurrence of MI beyond the Ginzburg–Landau approximation by considering the full T_2 dynamics. We introduce the theoretical framework in Section 2 and discuss the consequences for amplifiers in Section 3. There, we calculate the steady-state solutions and derive a dispersion relation for MI. The effect of the population relaxation damping time T_1 and the dipole dephasing time T_2 on MI are studied for amplifiers. We find that by cooling the fiber amplifier, the bandwidth and the strength of the MI can be greatly reduced. In Section 4 we deal with fiber lasers and derive the dispersion relation for MI at resonance. The role of saturable absorption in fiber lasers is investigated, and we focus on the possibility of MI occurring in the normal-dispersion regime. We find indeed such an instability, having its origin in the atomic coherence effects related to the atomic polarization dynamics. This new instability is found to occur at rather low frequencies (~50 MHz) and

0740-3224/97/102618-10$10.00

may explain the self-starting behavior of mode-locked Nd-doped lasers. In Section 5 we discuss the effects of detuning on the occurrence of MI and discuss the differences between normal and anomalous operating regimes.

2. THEORETICAL FRAMEWORK

Our starting point is a set of Maxwell–Bloch equations that describe the propagation of optical fields in a nonlinear, dispersive medium doped with two-level atoms (or ions). We write the electrical field $\mathscr{E}(x, y, z, t)$ and the induced material polarization $\mathscr{P}(x, y, z, t)$ as

$$\mathscr{E}(x, y, z, t) = \tfrac{1}{2}\,\hat{x}F(x, y)A(z, t) \times \exp[i(\beta_0 z - \omega_0 t)] + \text{c.c.}, \quad (1)$$

$$\mathscr{P}(x, y, z, t) = \tfrac{1}{2}\,\hat{x}F(x, y)B(z, t) \times \exp[i(\beta_0 z - \omega_0 t)] + \text{c.c.}, \quad (2)$$

where $\hat{x}$ is the polarization unit vector of the light assumed to be linearly polarized along the x axis, $F(x, y)$ is the fiber-mode profile, and β_0 is the wave number corresponding to the carrier frequency ω_0. We assume that the field-polarization direction is preserved upon propagation and that we are dealing with a polarization-preserving single-mode fiber. However, most of the results are expected to remain qualitatively valid for conventional optical fibers. After substituting Eqs. (1) and (2) into Maxwell's equations, and making the slowly-varying-envelope and rotating-wave approximations, we obtain the following equations for the slowly varying complex amplitudes A and B (Ref. 4):

$$\frac{\partial A}{\partial z} = \frac{i}{2}B - \frac{1}{2}\alpha A - \frac{i\beta_2}{2}\frac{\partial^2 A}{\partial t^2} + (\theta + i\gamma)|A|^2 A, \quad (3)$$

$$T_2\frac{\mathrm{d}B}{\mathrm{d}t} = (i\delta - 1)B - iAg, \quad (4)$$

$$T_1\frac{\mathrm{d}g}{\mathrm{d}t} = g_0 - g + \mathrm{Im}(A^* B)/P_{\mathrm{sat}}, \quad (5)$$

where g is the gain realized by pumping the dopants, α is the optical loss, β_2 is the GVD coefficient of the host fiber, θ accounts for saturable host absorption, γ is the fiber nonlinearity, $\delta = (\omega_0 - \bar{\omega})T_2$ is the scaled detuning between the carrier frequency ω_0 and the atomic resonance frequency $\bar{\omega}$, g_0 is the unsaturated gain, and P_{sat} is the saturation power for the dopants modeled as a homogeneously broadened two-level system. We have written Eqs. (3)–(5) in such a way that A has units of $\sqrt{W}$, B has units of $\sqrt{W}L^{-1}$, and g has units of L^{-1}, where L is the length of either the amplifier or the laser cavity.

It is important to note that Eqs. (3)–(5) are based on a traveling-wave description rather than a standing-wave approach that is employed in the conventional rate-equation analysis. Since we adopt a traveling-wave approach, the optical field $A(z, t)$ in Eqs. (3)–(5) in principle can represent a very wide spectrum (or many longitudinal modes). The detuning parameter δ is thus interpreted as the mismatch between the gain peak and the dominant frequency of the laser spectrum. The main assumptions in our model are the homogeneously broadened gain medium and the neglect of spontaneous emission. The former is not valid for all doped fibers, but for some types of glass hosts it is a reasonable assumption.[4] Since we are interested in deterministic instabilities, spontaneous emission can be neglected without loss of generality.

There are two distinct origins of the nonlinear effects in Eqs. (3)–(5). The fiber nonlinearity $\gamma = n_2\omega_0/cA_{\mathrm{eff}}$ accounts for SPM effects induced by the host, where n_2 is the nonlinear refractive index (units m^2/W), c is the speed of light in vacuum, and A_{eff} is the effective fibercore area. For completeness we give the relation between n_2 and the nonlinear susceptibility $\tilde{\chi}^{(3)}$ (units of meters squared per volt squared) of the fiber

$$n_2 \equiv \frac{3}{4\epsilon_0 n^2 c}\,\mathrm{Re}[\tilde{\chi}^{(3)}(\omega_0)], \quad (6)$$

where n is the background refractive index and ϵ_0 is the permittivity of the vacuum. The dopant-induced nonlinear effects are governed by the saturation power P_{sat}, defined as

$$P_{\mathrm{sat}} \equiv \frac{\hbar^2 c n \epsilon_0 A_{\mathrm{eff}}}{2\mu^2 T_1 T_2}, \quad (7)$$

where $\hbar$ is Planck's constant divided by 2π and μ is the dipole moment of the atomic transition. Note that Eqs. (3)–(5) are written in the frame of reference moving with group velocity $v_g \equiv \beta_1^{-1}$, which means that $t = T - \beta_1 z$, where T is the time in the rest frame. By doing this, we eliminate the term $\beta_1(\partial A/\partial T)$ from the left-hand side of Eq. (3).

We now briefly discuss the relation of Eqs. (3)–(5) with the CGL model.[4,12] When the assumption is made that the population relaxation time T_1 is much longer than all other lifetimes, we can approximate the actual gain g by its steady-state value g_s. This allows Eq. (4) to be expressed in the Fourier domain as the well-known Lorentzian-shaped nonlinear susceptibility:

$$\frac{\tilde{B}(\Delta\omega)}{\tilde{A}(\Delta\omega)} = \frac{-ig_s}{1 - i(\Delta\omega T_2 + \delta)}, \quad (8)$$

where $\Delta\omega = \omega - \omega_0$ is the detuning of the spectral component from the carrier frequency. In the CGL model, polarization equation (8) is approximated by a Taylor expansion near $\Delta\omega = 0$ up to second order, leading to the parabolic-gain approximation that is reasonably accurate for small values of T_2. In the time domain this corresponds to (generally complex) corrections $\Delta\beta_1$ and $\Delta\beta_2$ of the inverse group velocity β_1 and the GVD coefficient β_2 (Ref. 3):

$$\Delta\beta_1(\delta) = \frac{1}{2}g_2 T_2\frac{1}{(1 - i\delta)^2}, \quad (9)$$

$$\Delta\beta_2(\delta) = g_s T_2^2\frac{i}{(1 - i\delta)^3}. \quad (10)$$

From Eq. (9) we see that only at resonance ($\delta = 0$) can the resulting pulse propagation equation be written in the reference frame moving with the new group velocity (β_1

$+ \Delta\beta_1)^{-1}$, because only at resonance is the correction $\Delta\beta_1$ real. After writing the correction to the GVD as $\Delta\beta_2(0) = ib \equiv ig_s{T_2}^2$, the resulting equations of the CGL model become

$$\frac{\partial A}{\partial z} = \frac{1}{2}(g - \alpha)A + \frac{1}{2}(b - i\beta_2)\frac{\partial^2 A}{\partial t^2} + (\theta + i\gamma)|A|^2 A, \tag{11}$$

$$T_1 \frac{\mathrm{d}g}{\mathrm{d}t} = g_0 - g - \frac{g|A|^2}{P_{\mathrm{sat}}}. \tag{12}$$

Obviously, Eqs. (11) and (12) are good approximations of the full model only if T_1 is long enough and T_2 is short enough. In this paper we explore the shortcomings of the CGL model for realistic fiber lasers and amplifiers and find interesting behavior outside the realm of the CGL model. We note that the CGL model is only useful for amplifiers for which gain saturation can be neglected; otherwise, the gain dispersion b would be z dependent, which seems impractical at best.

The Maxwell–Bloch equations (3)–(5) can be applied to both amplifiers and unidirectional (e.g., ring) lasers. In the case of lasers, however, one should, in general, solve a complicated boundary-value problem to account for the localized losses at the cavity mirrors, a task that requires a numerical approach. In this paper we adopt the mean-intensity approximation by replacing the localized mirror losses with a distributed loss incorporated in the total optical loss α. In the case of amplifiers, such a mean-intensity requirement is not valid: the intensity is strongly z dependent. Because the steady states are so different for lasers and amplifiers, a modulation stability analysis yields very different results. In the following, we treat them separately.

3. MODULATION INSTABILITY IN AMPLIFIERS

We consider an amplifier (or absorber) of length L with an input power P_0 at $z = 0$. We first find the time-independent (steady-state) solution of Eqs. (3)–(5). Formally, it can be written as

$$A_s(z) = [P_A(z)]^{1/2}\exp[i\varphi_s(z)], \tag{13}$$

$$B_s(z) = \frac{A_s(z)g_s(z)}{\delta + i}, \tag{14}$$

$$g_s(z) = g_0\left[1 + \frac{P_A(z)}{P_{\mathrm{sat}}(1 + \delta^2)}\right]^{-1}. \tag{15}$$

Using the imaginary part of Eq. (3), we can write the phase profile $\varphi_s(z)$ in terms of the power profile $P_A(z)$:

$$\varphi_s(z) = \gamma\int_0^z \mathrm{d}z' P_A(z') + \frac{\delta/2}{1 + \delta^2}\int_0^z \mathrm{d}z' g_s(z'). \tag{16}$$

From the real part of Eq. (3), and using Eq. (15), one finds the following differential equation for the scaled power profile $f(z) \equiv P_A(z)/[P_{\mathrm{sat}}(1 + \delta^2)]$:

$$\frac{\mathrm{d}f}{\mathrm{d}z} = \frac{g_0}{1 + \delta^2}\frac{f}{f + 1} - \alpha f + 2\theta P_{\mathrm{sat}}(1 + \delta^2)f^2. \tag{17}$$

This differential equation can be solved, resulting in the following transcendental equation for P_A:

$$\begin{aligned} 2\theta P_{\mathrm{sat}}(1 + \delta^2)z &= -\left(\frac{C}{C_+} + \frac{1 - C}{C_-}\right)\ln\left[\frac{P_A(z)}{P_0}\right] \\ &\quad + \frac{C}{C_+}\ln\left[\frac{P_A(z) - C_+P_{\mathrm{sat}}(1 + \delta^2)}{P_0 - C_+P_{\mathrm{sat}}(1 + \delta^2)}\right] \\ &\quad + \frac{1 - C}{C_-}\ln\left[\frac{P_A(z) - C_-P_{\mathrm{sat}}(1 + \delta^2)}{P_0 - C_-P_{\mathrm{sat}}(1 + \delta^2)}\right], \end{aligned} \tag{18}$$

where the coefficients C and $C_\pm$ are given by

$$C = \frac{1 + C_+}{C_+ - C_-},$$

$$2C_\pm = c_2 - 1 \pm [(1 - c_2)^2 - 4(c_1 - c_2)]^{1/2}, \tag{19}$$

$$c_1 = \frac{g_0}{2\theta P_{\mathrm{sat}}(1 + \delta^2)^2}, \quad c_2 = \frac{\alpha}{2\theta P_{\mathrm{sat}}(1 + \delta^2)}. \tag{20}$$

In the absence of saturable absorption ($\theta = 0$), the solution of Eq. (17) is implicitly given by

$$\begin{aligned} \left(\frac{g_0}{1 + \delta^2} - \alpha\right)z &= \ln\left[\frac{P_A(z)}{P_0}\right] - \frac{g_0}{\alpha(1 + \delta^2)} \\ &\quad \times \ln\left\{\frac{P_A(z) - P_{\mathrm{sat}}(1 + \delta^2)\left[\dfrac{g_0}{\alpha(1 + \delta^2)} - 1\right]}{P_0 - P_{\mathrm{sat}}(1 + \delta^2)\left[\dfrac{g_0}{\alpha(1 + \delta^2)} - 1\right]}\right\}, \end{aligned} \tag{21}$$

which, in the absence of optical loss ($\alpha = 0$), reduces to

$$\ln\left[\frac{P_A(z)}{P_0}\right] + \frac{P_A(z) - P_0}{P_{\mathrm{sat}}} = \frac{g_0 z}{1 + \delta^2}. \tag{22}$$

After the power profile $P_A(z)$ is found, the gain profile $g_s(z)$ and the polarization profile $B_s(z)$ follow from Eqs. (13)–(16).

To study the onset of MI, we follow a standard approach[4] by considering the linear stability of the steady-state (cw) solution given above. Considering small perturbations u, v, p, q, and x from the cw state defined as

$$A(z,t) = [(P_0)^{1/2} + u(z,t) + iv(z,t)] \times \left[\frac{P_A(z)}{P_0}\right]^{1/2} \exp[i\varphi_s(z)], \tag{23}$$

$$B(z,t) = \frac{g_s(z)}{\delta + i}[(P_0)^{1/2} + p(z,t) + iq(z,t)] \times \left[\frac{P_A(z)}{P_0}\right]^{1/2} \exp[i\varphi_s(z)], \tag{24}$$

$$g(z,t) = [g_0 + x(z,t)]\left[1 + \frac{P_A(z)}{P_{\text{sat}}(1+\delta^2)}\right]^{-1}, \tag{25}$$

and linearizing Eqs. (3)–(5) in u, v, p, q, and x, we solve the resulting five linear equations in Fourier space by introducing

$$y(z,t) = y_0 \exp\left[i\int \mathrm{d}zK(z) - i\Omega t\right], \qquad y = u, v, p, q, x, \tag{26}$$

where y_0 is the initial amplitude, Ω is the frequency, and $K(z)$ is the local wave number of the perturbation. The resulting dispersion relation for arbitrary detuning δ is discussed for fiber lasers in Section 5. The dispersion relation at resonance ($\delta = 0$) is given by

$$\begin{aligned}\{&[2iK(z) + g_s(z) - 4\theta P_A(z)][2iK(z) + g_s(z)] \\ &+ \beta_2{}^2\Omega^2[\Omega^2 + \mathrm{sgn}(\beta_2)\Omega_c{}^2(z)]\}(1 - i\Omega T_2) \\ &\times [(1 - i\Omega T_1)(1 - i\Omega T_2) + I(z)] \\ &- g_s(z)[2iK(z) + g_s(z)](1 - i\Omega T_2) \\ &\times [1 - i\Omega T_1 - I(z)] - g_s(z) \\ &\times [2iK(z) + g_s(z) - 4\theta P_A(z)] \\ &\times [(1 - i\Omega T_1)(1 - i\Omega T_2) + I(z)] \\ &+ g_s{}^2(z)[1 - i\Omega T_1 - I(z)] = 0,\end{aligned} \tag{27}$$

where $I(z) = P_A(z)/P_{\text{sat}}$, $\mathrm{sgn}(\beta_2) = \pm 1$, and $\Omega_c(z) = [4\gamma P_A(z)/|\beta_2|]^{1/2}$ is the critical frequency, i.e., the maximum frequency for which MI is found to occur in the case of anomalous dispersion in a passive fiber.[4] Before we examine the implications of Eq. (27) in various regimes of parameter space, we note that the Rabi frequency is somewhat hidden:

$$\Omega_{\text{Rabi}}(z) \equiv \left[\frac{P_A(z)}{P_{\text{sat}}T_1T_2}\right]^{1/2}. \tag{28}$$

The imaginary part of $K(z)$ determines the local gain experienced by the perturbation. It is useful to define the total integrated gain at frequency Ω as[11]

$$h(\Omega) \equiv -2\int_0^L \mathrm{d}z\ \mathrm{Im}[K(\Omega, z)], \tag{29}$$

where the factor 2 converts $h(\Omega)$ to power gain. MI occurs whenever the wave number K has a negative imaginary part. In the case of an amplifier, this means the perturbation grows faster than the steady-state power, whereas for an absorber it means that the perturbation dampens less quickly. Dispersion equation (27) reduces to the previously reported ones in the appropriate limits. In the absence of saturable host absorption ($\theta = 0$), the dispersion relation from Ref. 11 is obtained in the limit of large T_1 and short T_2.

We now consider the occurrence of MI in various regimes of parameter space for both amplifiers and absorbers. Because our model has no restrictions with respect to the magnitude of the lifetimes T_1 and T_2, we can explore MI in regimes where the CGL model has no validity. For simplicity, we only consider the local perturbation gain because the integration in Eq. (29) can be performed analytically in a few limiting cases only.[3] We also ignore the possibility of saturable host absorption since two-photon absorption is relatively weak in silica fibers, and other sources of saturable nonlinearity are rarely present in amplifiers. When we discuss MI in lasers, we show how even relatively small amounts of saturable host absorption can affect the MI drastically.

We start by investigating the effect of the magnitude of the dipole lifetime T_2. For most fiber amplifiers, T_2 is estimated to be near 100 fs, corresponding to a wide gain spectrum. Because T_1 is usually in the range 0.1–10 ms, the CGL equation is expected to be a good approximation. However, by cooling the fiber, the polarization dephasing process can be slowed down substantially, making values of $T_2 \sim 10$ ps readily attainable.[13]

In Fig. 1 we show for various values of T_2 in the range 0.1–10 ps the MI spectrum for a typical fiber amplifier with a 30-dB gain, i.e., $\exp(g_0L) = 1000$. All other parameters are given in the caption. Note that the saturation power P_{sat} is inversely proportional to T_2 [Eq. (7)]. When Eq. (7) is satisfied for each value of T_2, the Rabi frequency remains a constant for all curves: $\Omega_{\text{Rabi}} = 1.29 \times 10^{-3}\Omega_c$. When the dephasing time T_2 is increased, two trends are observed.

First, as can be seen in Fig. 1, increasing T_2 leads to a shrinkage of the MI bandwidth, whereas the maximum

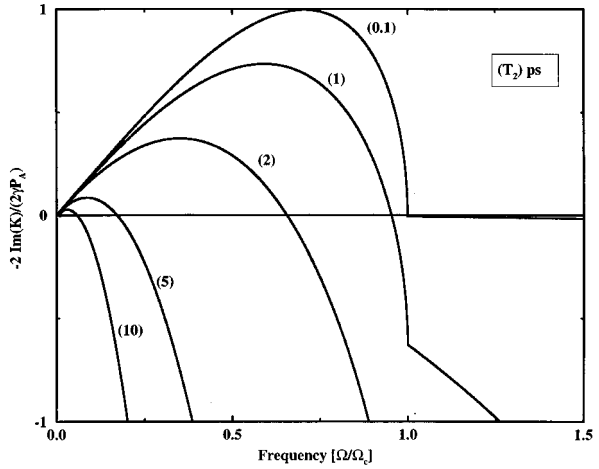

Fig. 1. Modulation instability spectrum for an erbium-doped fiber amplifier at various values of T_2 (indicated in the figure). Parameters are $g_0 = 6.91\,\mathrm{L}^{-1}$, $P_0 = 1$ mW, $T_1 = 0.1$ ms, $\beta_2 = -20\,\mathrm{ps}^2/\mathrm{L}$, $\gamma = 3W^{-1}\,\mathrm{L}^{-1}$, and $P_{\text{sat}} = 1$ mW when $T_2 = 0.1$ ps. For undoped fibers, MI occurs up to $\Omega_{\text{crit}}/2\pi = 3.9$ GHz

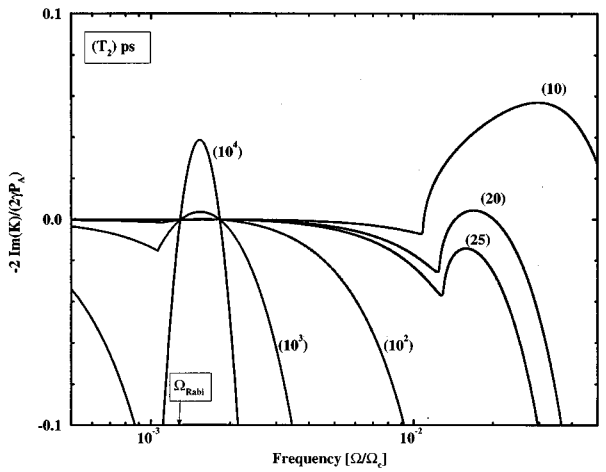

Fig. 2. MI spectrum for the amplifier of Fig. 1, for even longer dephasing times T_2 (indicated in the figure). In the range 21 $< T_2 <$ 80 ps, MI is totally quenched. When T_2 approaches 100 ps, the MI spectrum starts to show a narrow, weak peak around the Rabi frequency $\Omega_{\mathrm{Rabi}}/\Omega_c = 0.0013$.

gain within the bandwidth decreases rapidly. When $T_2 = 100$ fs ($P_A/P_{\mathrm{sat}} = 0.01$), MI occurs for frequencies up to $\Omega_c/2\pi = 3.9$ GHz, while the peak MI strength is found near $\Omega = \Omega_c/\sqrt{2}$. The peak strength is very close to the analytical value $2\gamma P_A$, which is found in the CGL limit.[11] Already when $T_2 = 2$ ps ($P_A/P_{\mathrm{sat}} = 0.2$), the frequency band where MI occurs has shrunk ~40%, and near $T_2 = 8$ ps ($P_A/P_{\mathrm{sat}} = 0.8$), MI has almost ceased to occur at all. Near $T_2 = 21$ ps ($P_A/P_{\mathrm{sat}} = 2.1$), the MI band vanishes completely. Long before that happens, the strength of MI is so weak that it is doubtful whether it can be observed in a single-pass amplifier.

Second, during this MI spectrum shrinkage, another phenomenon is occurring that is directly caused by the two-level system since it involves frequencies close to Ω_{Rabi}, as is shown in Fig. 2. Near the Rabi frequency a secondary, weak maximum in MI strength begins to form for $T_2 > 20$ ps. This maximum becomes positive near $T_2 = 80$ ps ($P_A/P_{\mathrm{sat}} = 8$) and grows with T_2. When T_2 is increased further, the MI spectrum slowly returns to its original width and strength (out of scale in Fig. 2). Near $T_2 = 11.5$ ns ($P_A/P_{\mathrm{sat}} = 1150$), the MI spectrum shows again positive MI gain around Ω_c, while maintaining a narrow (but weak) peak close to Ω_{Rabi}. At the highly improbable value of $T_2 \sim 1\ \mu$s ($P_A/P_{\mathrm{sat}} = 10^5$) the MI spectrum is very close to the one at $T_2 = 100$ fs, and we have come full circle.

Thus we find four regimes of T_2; in the first regime (100 fs $< T_2 <$ 21 ps), increasing T_2 leads to a total quenching of MI. In the second regime (21 ps $< T_2 <$ 80 ps), no MI occurs, but the gain around the Rabi frequency is growing. In the third regime (80 ps $< T_2 <$ 11.5 ns), more and more MI occurs around the Rabi frequency, while the gain around Ω_c is growing toward a positive value again. In the fourth regime, approaching the long T_2 limit (1 μs $< T_2 < \infty$), the MI spectrum recovers fully to its original (small T_2) form. The boundaries between these regimes are, of course, strongly dependent on the power level P_A. For higher power levels these boundaries rapidly decrease.

We further note that the MI band near Ω_c is insensitive to changes in T_1, as long as it is accompanied by a change in the saturation power P_{sat} according to Eq. (7). However, if we keep the saturation power constant upon changing T_1 (this can be done by adjusting the dipole moment μ), decreasing T_1 leads to a stabilization of the lower frequencies and eventually a reduction of MI altogether.

We emphasize that the narrow MI peak around Ω_{Rabi} is so weak that it is questionable whether it can be observed in an amplifier. In the case of a laser, however, such a weak gain may build to a substantial instability over many round trips, as we discuss in the next section. Since it is not common to use an amplifier in the highly saturated regime, the emergence of the narrow MI band near the Rabi frequency is not very practical. Note, however, that this narrow MI band near the Rabi frequency does not depend on the sign of β_2; in both normal- and anomalous-dispersion regimes, this instability emerges at relatively high values of T_2.

Apart from this new (and for realistic systems, extremely weak) instability, the full Maxwell–Bloch model agrees with the CGL model qualitatively rather well. Of course, the quantitative differences become larger as the approximations leading to the CGL model (large T_1 and short T_2) become more and more inappropriate. In the next section we find that for lasers the situation can be very different.

4. MODULATION INSTABILITY IN FIBER LASERS AT RESONANCE

Equations (3)–(5) also describe the optical field and the gain in a laser, when one assumes that all losses can be thought of as being distributed along the cavity. Then, the steady-state solution is characterized by a z-independent power P_0 and gain g_s, and can be written as

$$A_s(z) = (P_0)^{1/2} \exp[i\varphi_s(z)], \tag{30}$$

$$B_s(z) = \frac{\delta - i}{1 + \delta^2} A_s g_s, \tag{31}$$

$$g_s = g_0\left[1 + \frac{P_0}{P_{\mathrm{sat}}(1 + \delta^2)}\right]^{-1}. \tag{32}$$

Again, from the real and the imaginary part of Eq. (3), the following expressions for the laser power P_0 and the phase profile $\varphi_s(z)$ are obtained:

$$g_s = (\alpha - 2\theta P_0)(1 + \delta^2), \tag{33}$$

$$\frac{\mathrm{d}\varphi_s}{\mathrm{d}z} = \gamma P_0 + \frac{1}{2}\left(\frac{\delta g_s}{1 + \delta^2} - \alpha\right). \tag{34}$$

Since Eq. (33) is quadratic in P_0 [with use of Eq. (32)], in principle, two values for the laser power are found. One of these is not physical and corresponds to the antilaser, which is characterized by a huge gain and almost zero power.

Similar to the amplifier case, we consider small perturbations u, v, p, q, and x from the cw state, defined as

$$A(z, t) = [(P_0)^{1/2} + u(z, t) + iv(z, t)]\exp[i\varphi_s(z)], \quad (35)$$

$$B(z, t) = \frac{\delta - i}{1 + \delta^2}[(P_0)^{1/2} + p(z, t) + iq(z, t)]g_s\exp[i\varphi_s(z)], \quad (36)$$

$$g(z, t) = [g_0 + x(z, t)]\left[1 + \frac{P_0}{P_{\text{sat}}(1 + \delta^2)}\right]^{-1}, \quad (37)$$

and linearizing Eqs. (3)–(5) in u, v, p, q, and x, we solve the resulting five linear equations in the Fourier space by introducing

$$y(z, t) = y_0 \exp[i(Kz - \Omega t)], \qquad y = u, v, p, q, x, \quad (38)$$

where y_0 denotes the initial amplitude of the perturbation. Note that because because both laser power P_0 and g_s are z independent, the wave number K is also z independent. At resonance ($\delta = 0$), the resulting dispersion relation reads

$$\begin{aligned}\{&[2iK + \alpha - 6\theta P_0](2iK + \alpha - 2\theta P_0) \\ &+ \beta_2{}^2\Omega^2[\Omega^2 + \text{sgn}(\beta_2)\Omega_c{}^2]\}(1 - i\Omega T_2) \\ &\times [(1 - i\Omega T_1)(1 - i\Omega T_2) + I_0] \\ &- g_s(2iK + \alpha - 2\theta P_0)(1 - i\Omega T_2) \\ &\times [1 - i\Omega T_1 - I_0] - g_s(2iK + \alpha - 6\theta P_0) \\ &\times [(1 - i\Omega T_1)(1 - i\Omega T_2) + I_0] \\ &+ g_s{}^2(1 - i\Omega T_1 - I_0) = 0. \end{aligned} \quad (39)$$

Here, $I_0 = P_0/P_{\text{sat}}$, $\text{sgn}(\beta_2) = \pm 1$, and $\Omega_c = (4\gamma P_0/|\beta_2|)^{1/2}$ is the critical frequency, i.e., the maximum frequency for which MI is found in the case of anomalous dispersion in a passive fiber.[4] This dispersion relation is identical to Eq. (27) when one replaces K, P_0, and g_s by their z-dependent counterparts, and Eq. (33) is used.

Dispersion relation (39) reduces to the one previously reported by Chen *et al.*,[12] who employ the CGL model, in the appropriate limit.

Before we proceed with examining the implications of Eq. (39) in various regimes of parameter space, we note that the Rabi frequency is now given by

$$\Omega_{\text{Rabi}} \equiv \left(\frac{P_0}{P_{\text{sat}}T_1T_2}\right)^{1/2}. \quad (40)$$

Merely comparing the relative strengths of the critical frequency Ω_c with the Rabi frequency Ω_{Rabi} does not provide much information about the effect of atomic coherence on MI. The interaction between the fiber nonlinearity, the GVD, and the two-level system is much more involved.

In contrast with the amplifier case described in the previous section, lasers generally operate in the heavily saturated regime. This means that the instability near the Rabi frequency is now more likely to play a significant role. Furthermore, many fiber laser systems, e.g., a figure-eight laser, contain an effective saturable absorber that causes mode locking.

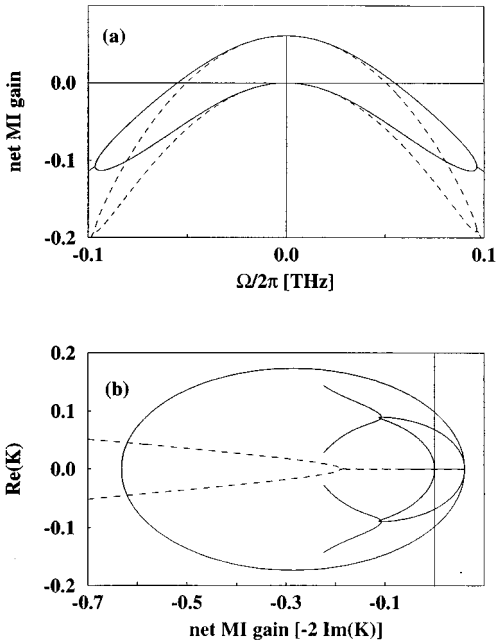

Fig. 3. MI analysis for a figure-eight laser. Solid curves indicate the results of the full model, while dashed curves show those of the CGL model. Top figure shows the net MI gain spectra, while the bottom figure shows the corresponding trajectory of the eigenvalue K on the complex plane. Parameters are $\alpha = 0.4\ \text{L}^{-1}$, $g_0 = 6\ \text{L}^{-1}$, $\beta_2 = -0.09\ \text{ps}^2\,\text{L}^{-1}$, $\theta = 0.1\ \text{W}^{-1}\,\text{L}^{-1}$, $\gamma = 0.008\ \text{W}^{-1}\,\text{L}^{-1}$, $T_2 = 1.27$ ps, $T_1 = 10^8$ ps, and $P_{\text{sat}} = 10$ mW.

We first compare the predictions of Eq. (39) with the CGL-based expression.[12] To facilitate comparison, we used the same parameters as in Ref. 12. In Fig. 3 we show the differences for the case of a figure-eight laser. Although the trajectories of K in the complex plane as a function of frequency Ω are quite different for a figure-eight laser, the resulting net MI gain spectra agree quite well, at least in the central region. The frequency range over which positive net MI gain occurs is underestimated by 10% by the CGL model. Both models show vanishing gain at 100 kHz [indicated by the vertical line at $\Omega \sim 0$ in Fig. 3(a)], whereas the frequency with highest gain is near 200 kHz. The Rabi frequency in this case is $\Omega_{\text{Rabi}} = 55$ MHz, and the critical frequency is $\Omega_c = 37$ GHz. They differ by almost three orders of magnitude. Even so, MI occurs for frequencies almost twice as large as Ω_c.

The results for the dye-laser parameters are shown in Fig. 4. Our model predicts that MI occurs in a narrow band near 30 GHz, whereas the CGL model predicts no instability at all! The Rabi frequency Ω_{Rabi} and the critical frequency Ω_c are both close to 24 GHz, which explains why the interaction between the fiber and the two-level system is so highly nonlinear.

Here we find the first meaningful qualitative difference between the full Maxwell–Bloch model and the CGL model. Not surprisingly, the laser power in Fig. 4 is ~60 times the saturation power P_{sat}, which makes the Rabi frequency of the same order as the critical frequency Ω_c.

So for the dye laser of Fig. 4 the interaction between the two-level system on the one side and the GVD and the SPM on the other side cannot be described within a parabolic-gain approximation.

The pump value g_0 at which the cw state loses its stability is often classified as the second threshold,[1] as it announces the onset of unstable behavior. Similarly, we can identify the MI threshold as the gain above which MI occurs. At this threshold, MI occurs only at the frequency corresponding to the peak gain in the MI spectrum, which can be compared with the frequency with which perturbations grow at a Hopf bifurcation. In Figs. 5 and 6 we show the dependence of the MI threshold as a function of θ for the case of the figure-eight laser (Fig. 5) and the dye laser (Fig. 6). The effect of saturable absorption is very dramatic in the case of the figure-eight laser

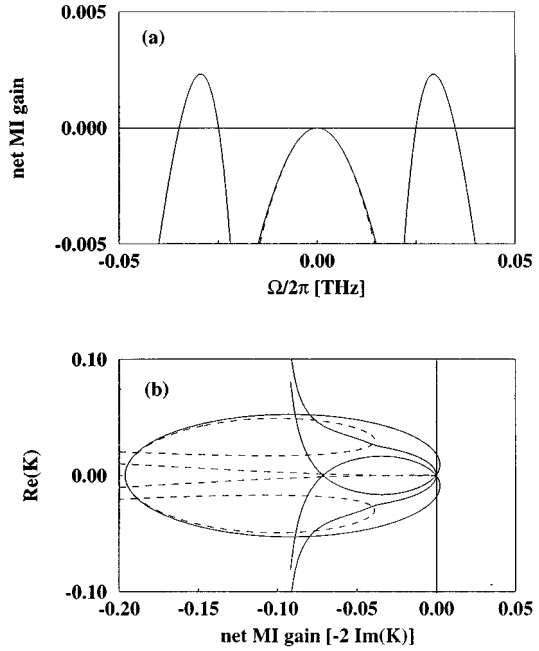

Fig. 4. MI analysis for a dye laser. Similar as in Fig. 3, except for the parameters: $\alpha = 0.1\,\mathrm{L}^{-1}$, $g_0 = 3\,\mathrm{L}^{-1}$, $\beta_2 = -0.09\,\mathrm{ps}^2\,\mathrm{L}^{-1}$, $\theta = 0.001\,\mathrm{W}^{-1}\,\mathrm{L}^{-1}$, $\gamma = 0.008\,\mathrm{W}^{-1}\,\mathrm{L}^{-1}$, $T_2 = 2.45$ ps, $T_1 = 10^3$ ps, and $P_{\mathrm{sat}} = 1$ mW.

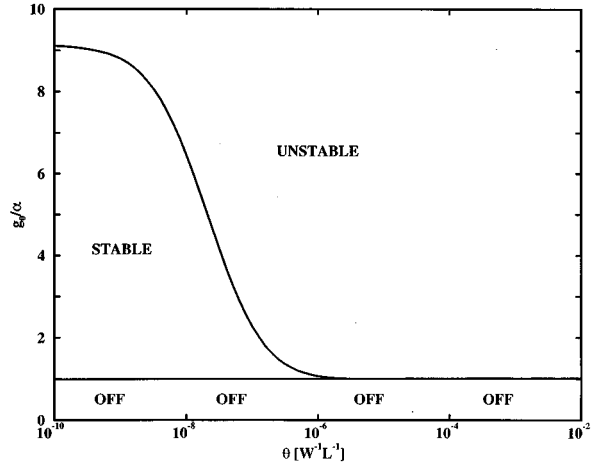

Fig. 5. MI threshold as a function of saturable absorption θ for the fiber laser of Fig. 3.

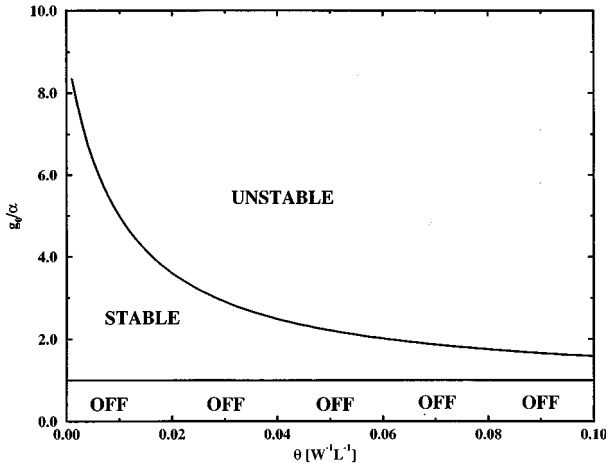

Fig. 6. MI threshold as a function of saturable absorption θ for the dye laser of Fig. 4.

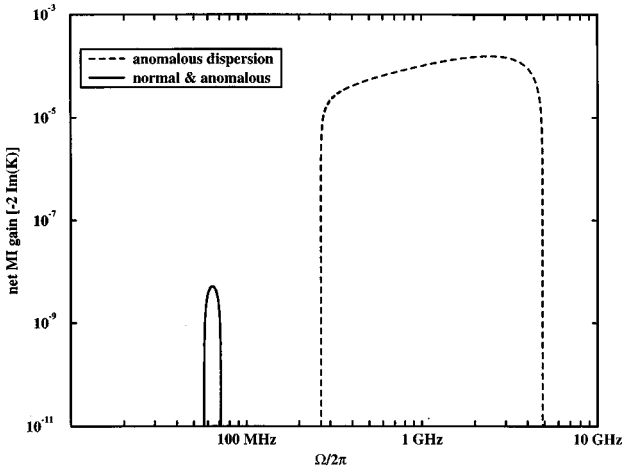

Fig. 7. Comparison of net MI gain spectra in the absence of saturable absorption ($\theta = 0$), for the cases of normal and anomalous dispersion. Other parameters of the fiber laser are the same as in Fig. 3.

parameters: when θ is larger than $10^{-6}\mathrm{W}^{-1}\mathrm{L}^{-1}$. MI occurs immediately after the first (lasing) threshold. A qualitatively similar dependence is found for the dye laser, where the MI threshold gain decreases from ~ 9 to 1.5 at $\theta = 0.1$. This feature explains why a relatively weak saturable absorber can lead to passive mode locking. Although the presence of a saturable absorber is evidently very useful for the generation of mode-locked pulses, it somewhat obscures our investigation of the interaction between the two-level system and the fiber nonlinearity and dispersion. This explains why for both the figure-eight laser and the dye laser of Figs. 3 and 4, the results hardly change if we consider normal dispersion.

We therefore examine the case $\theta = 0$, so that we can consider the sole interaction between the fiber nonlinearity and the two-level system occurring in the absence of saturable absorption. The interesting question is whether atomic coherence can lead to MI in the normal-dispersion regime of the fiber. According to the CGL model, this is not possible.

In Fig. 7 we show, again for a fiber laser, but without saturable absorption (ring-cavity instead of figure-eight

geometry), the net MI gain spectra for $\beta_2 = \pm 0.09\ \mathrm{ps}^2\ \mathrm{L}^{-1}$. For anomalous dispersion, we find an approximately 4-GHz-wide MI band centered near 2.5 GHz and a much narrower and much weaker MI band centered near 50 MHz. While the MI band near 2.5 GHz vanishes in the case of normal dispersion, the narrow low-frequency band survives. So, contrary to what the CGL model predicts, the presence of dopants can cause MI instability in the normal-dispersion regime of the fiber. Furthermore, in contrast to the amplifier case (Section 2), any positive value of $-2\,\mathrm{Im}(K)$ should be taken seriously, since, in a laser, even the smallest growth of a perturbation may cause a significant change in the output signal after many round trips in the cavity.

Figure 8 shows the peculiar dependence of this new MI at normal dispersion when the population relaxation time T_1 is decreased from 10 μs to 1.375 μs. Upon decreasing T_1, the new MI band initially grows stronger, while shifting to higher frequencies. Decreasing T_1 further causes the band to weaken and finally to vanish abruptly at $\sim$1.35 μs.

We stress that our results indicate that a fiber ring laser, operating in the normal-dispersion regime, may show unstable behavior at high pump levels, even in absence of additional saturable absorbing mechanisms. At resonance, the strength of the MI in the normal-dispersion regime is rather weak, which would imply that the instability needs to build up during many round trips in the ring laser. In the next section we discuss the effect of detuning on the strength and the nature of this new instability.

5. MODULATION INSTABILITY IN DETUNED FIBER LASERS

With various experimental techniques, e.g., through the use of gratings, one can force a fiber laser to operate away from the gain peak. In our theory this means that we have to deal with the effect of detuning δ. Recall that there is no CGL version for the detuned case, as the group velocity becomes complex in the parabolic-gain approximation. For arbitrary detuning, dispersion relation Eq. (39) reads

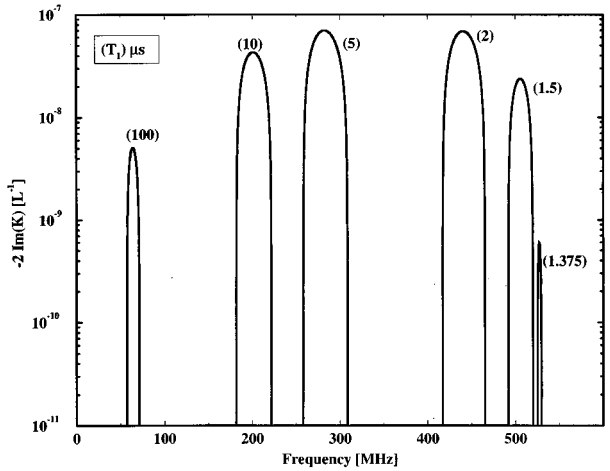

Fig. 8. New MI band at normal dispersion as a function of population relaxation time T_1 (indicated). Other parameters of the fiber laser are the same as those in Fig. 3.

$$
\begin{aligned}
&\left[\left(2iK + \frac{g_s}{1+\delta^2} - 4\theta P_0\right)\left(2iK + \frac{g_s}{1+\delta^2}\right)\right.\\
&\quad\left. + \left(\beta_2\Omega^2 - \frac{\delta g_s}{1+\delta^2}\right)\left(\beta_2\Omega^2 + 4\gamma P_0 - \frac{\delta g_s}{1+\delta^2}\right)\right]\\
&\quad\times\{(1 - i\Omega T_2)[(1 - i\Omega T_1)(1 - i\Omega T_2) + I_0]\\
&\quad + \delta^2(1 - i\Omega T_1)\} + \frac{-g_s}{1+\delta^2}\left(2iK + \frac{g_s}{1+\delta^2}\right)\\
&\quad\times\left[(1 - i\Omega T_1)(1 - i\Omega T_2)\right.\\
&\quad\left. - \left(1 - \frac{i\Omega T_2}{1+\delta^2}\right)I_0 + \delta^2(1 - i\Omega T_1)\right]\\
&\quad + \frac{-g_s}{1+\delta^2}\left(2iK + \frac{g_s}{1+\delta^2} - 4\theta P_0\right)\\
&\quad\times\left[(1 - i\Omega T_1)(1 - i\Omega T_2) + \left(1 - \frac{i\Omega T_2\delta^2}{1+\delta^2}\right)I_0\right.\\
&\quad\left. + \delta^2(1 - i\Omega T_1)\right] + \frac{{g_s}^2}{1+\delta^2}\\
&\quad\times[(1+\delta^2)(1 - i\Omega T_1) - I_0]\\
&\quad + 2i\Omega T_2 g_s\frac{\delta^2}{1+\delta^2}\left(2iK + \frac{g_s}{1+\delta^2} - 2\theta P_0\right)\\
&\quad\times\left[1 - i\Omega T_1 - \frac{I_0}{(1+\delta^2)}\right]\\
&\quad + \frac{\delta g_s}{1+\delta^2}\left(\beta_2\Omega^2 - \frac{\delta g_s}{1+\delta^2}\right)\\
&\quad\times[(1+\delta^2)(1 - i\Omega T_1) - I_0]\\
&\quad + \frac{\delta g_s}{1+\delta^2}\left(\beta_2\Omega^2 + 4\gamma P_0 - \frac{\delta g_s}{1+\delta^2}\right)\\
&\quad\times[(1+\delta^2)(1 - i\Omega T_1) + (1 - i\Omega T_2)I_0] = 0, \quad (41)
\end{aligned}
$$

where $I_0 = P_0/P_{\mathrm{sat}}$. Equation (39) is recovered by putting $\delta = 0$ and $g_s = \alpha - 2\theta P_0$. Equation (41) can be applied as well for amplifiers by treating P_0, g_s, and K as z-dependent quantities.

We now use Eq. (41) to investigate the effect of detuning on the MI spectra shown in Fig. 7. The introduction of δ into the problem makes the situation even more complex. Instead of only two frequencies, i.e., the critical frequency Ω_c and the Rabi frequency Ω_{Rabi}, the problem now is governed by the interaction of three frequencies. In Figs. 9 and 10 we show the effect of detuning on the bandwidth and the strength of MI for normal and anomalous dispersion, respectively. Clearly, small detunings have a large effect on the occurrence of MI, and the sign of the detuning also matters. This spectral asymmetry is due to the fiber host nonlinearities. When GVD and SPM are absent, Eq. (41) is symmetric in detuning δ. In the anomalous-dispersion regime (Fig. 10), a small value of the detuning connects the two MI bands, one owing to

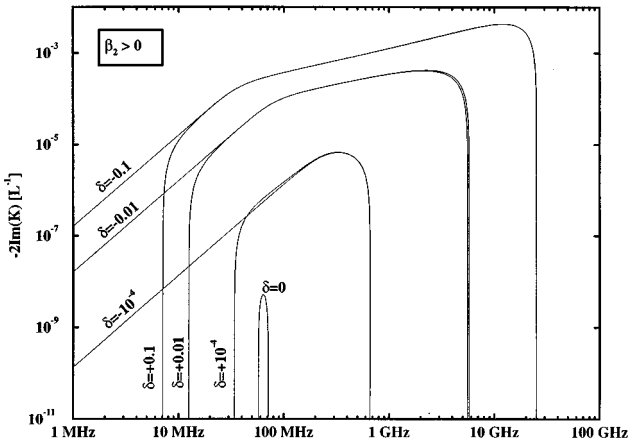

Fig. 9. Effect of detuning on the new MI in the normal-dispersion regime. Parameters identical to those in Fig. 7.

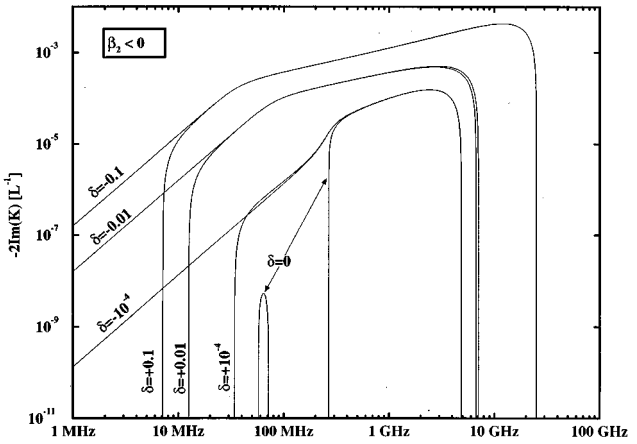

Fig. 10. Similar to Fig. 9, except that the laser now operates in the anomalous-dispersion regime.

the passive fiber MI and the other owing to two-level dynamics. Upon increasing the absolute value of the detuning, the MI bandwidth and the strength increase logarithmically. At large detuning ($\delta = 0.1$), there is no distinction between the normal- and anomalous-dispersion case. For large detuning the instability is apparently dominated by the two-level dynamics.

6. CONCLUSIONS

We have analyzed the occurrence of modulation instability (MI) in fiber lasers and amplifiers by considering the self-phase modulation, group-velocity dispersion, and the saturable host absorption. The gain spectrum has been fully considered, in contrast to the parabolic-gain approximation employed in the complex Ginzburg–Landau (CGL) model. We have derived analytical expressions for the MI dispersion $K(\Omega)$ that naturally reduce to previously reported research for both lasers and amplifiers.

For amplifiers, operating not too heavily saturated and in absence of saturable absorption, no qualitative differences with the CGL description are found, even in regimes where the basic approximations of that model are violated. Quantitatively, however, the differences can be quite substantial. We show that by cooling the fiber amplifier and thereby increasing the dipole dephasing time, the occurrence of MI can be quenched. For heavily saturated amplifiers, we find a new instability located in a narrow frequency band around the Rabi frequency. The CGL model does not predict such an instability. The strength of this new instability is very small, and it is questionable that its effect can be detected in a single-pass amplifier.

In lasers, a different picture emerges, since any growing perturbation may build up over many round trips within the laser cavity. Furthermore, the presence of a weakly saturable absorbing mechanism is shown to greatly enhance the instability. We compare our results with those of Chen *et al.*,[12] who used the CGL model to investigate MI in a dye laser and a figure-eight laser.[12] Our results for the figure-eight laser agree rather well, whereas we find disagreement for the dye laser, which in our model is predicted to have an instability of ~30 GHz. Further indication that the CGL model should be used with caution is given when systems without saturable absorption are studied: for a fiber ring laser operating in the normal-dispersion regime, a narrow MI band of low (~50-MHz) frequencies is found, which is not predicted by the CGL model. This may explain the self-starting of mode-locked Nd-doped fiber lasers.

The effect of detuning on the strength and the bandwidth of the new instability can be substantial, since nonzero detuning effectively introduces a new frequency into the problem. Even for a relatively small detuning, the strength and the bandwidth of MI increase logarithmically, whereas the difference between normal and anomalous dispersion becomes smaller. The fiber nonlinearities cause the MI spectrum to become asymmetric with respect to detuning.

ACKNOWLEDGMENTS

This work was supported in part by the NASA Ames Research Center, the U.S. Army Research Office, and the National Science Foundation under grant PHY94-15583. Helpful discussions with Peter Goorjian are also acknowledged.

REFERENCES

1. C. O. Weiss and R. Vilaseca, *Dynamics of Lasers* (Weinheim, New York, 1991).
2. G. H. M. van Tartwijk and G. P. Agrawal, "Nonlinear dynamics in the generalized Lorenz–Haken model," Opt. Commun. **133**, 565–577 (1997).
3. G. P. Agrawal, "Optical pulse propagation in doped fiber amplifiers," Phys. Rev. A **44**, 7493–7501 (1991).
4. G. P. Agrawal, *Nonlinear Fiber Optics*, 2nd ed. (Academic, New York, 1995).
5. F. Sanchez and G. Stephan, "General analysis of instabilities in erbium-doped fiber lasers," Phys. Rev. E **53**, 2110–2122 (1996).
6. S. Colin, E. Contesse, P. Le Boudec, G. Stephan, and F. Sanchez, "Evidence of a saturable-absorption effect in heavily erbium-doped fibers," Opt. Lett. **21**, 1987–1989 (1996).
7. E. Lacot, F. Stoeckel, and M. Chenevier, "Self pulsing,

chaos and antiphase dynamics in an Er^{3+} doped fiber laser," J. Phys. (France) III **5**, 269–279 (1995).
8. Q. L. Williams and R. Roy, "Fast polarization dynamics of an erbium-doped fiber ring laser," Opt. Lett. **21**, 1478–1480 (1996).
9. S. Bielawski, D. Derozier, and P. Glorieux, "Antiphase dynamics and polarization effects in the Nd-doped fiber laser," Phys. Rev. A **46**, 2811–2822 (1992).
10. H. Zeghlache and A. Boulnois, "Polarization instability in lasers. I. Model and steady states of neodymium-doped fiber lasers," Phys. Rev. A **52**, 4229–4242 (1995); "Polarization instability in lasers: II: Influence of the pump polarization on the dynamics," Phys. Rev. A **52**, 4243–4254 (1995).
11. G. P. Agrawal, "Modulation instability in erbium-doped fiber amplifiers," IEEE Photonics Technol. Lett. **4**, 562–564 (1992).
12. C.-J. Chen, P. K. A. Wai, and C. R. Menyuk, "Self-starting of passively mode-locked lasers with fast saturable absorbers," Opt. Lett. **20**, 350–352 (1995).
13. M. Nakazawa, K. Suzuki, Y. Kimura, and H. Kubota, "Coherent π-pulse propagation with pulse breakup in an erbium-doped fiber waveguide amplifier," Phys. Rev. A **45**, R2682–R2685 (1992).